Article

Cell Chemical Biology

Small-Molecule Protein-Protein Interaction Inhibitor of Oncogenic Rho Signaling

Highlights

- Uncontrolled activation of Rho signaling by AKAP13 RhoGEF is tumorigenic
- A hot region for RhoA recognition and activation by AKAP13 was identified
- Virtual screening discovered an inhibitor of AKAP13-RhoA interaction
- The compound inhibits oncogenic AKAP13 signals and reverses cancer cell phenotypes

Authors

Dario Diviani, Francesco Raimondi, Cosmo D. Del Vescovo, ..., Luca Bellucci, Michele Seeber, Francesca Fanelli

Correspondence

fanelli@unimo.it

In Brief

Diviani et al. found a "hot" region for RhoA recognition and activation by Lbc. Virtual screening of compounds targeting that region discovered an inhibitor of Lbc-RhoA interaction able to halt oncogenic Lbc signals and reverse cancer cell phenotypes.

Diviani et al., 2016, Cell Chemical Biology *23*, 1135–1146
September 22, 2016
http://dx.doi.org/10.1016/j.chembiol.2016.07.015

Please cite this article as: Diviani et al., Small-Molecule Protein-Protein Interaction Inhibitor of Oncogenic Rho Signaling, Cell Chemical Biology (2016), http://dx.doi.org/10.1016/j.chembiol.2016.07.015

Cell Chemical Biology
Article

Small-Molecule Protein-Protein Interaction Inhibitor of Oncogenic Rho Signaling

Dario Diviani,[1] Francesco Raimondi,[2] Cosmo D. Del Vescovo,[1] Elisa Dreyer,[1] Erica Reggi,[1] Halima Osman,[1] Lucia Ruggieri,[1] Cynthia Gonano,[1] Sabrina Cavin,[1] Clare L. Box,[3] Marc Lenoir,[3] Michael Overduin,[4] Luca Bellucci,[2] Michele Seeber,[2] and Francesca Fanelli[2,5,*]

[1]Department of Pharmacology and Toxicology, Faculty of Biology and Medicine, University of Lausanne, Rue du Bugnon 27, 1005 Lausanne, Switzerland
[2]Department of Life Sciences, University of Modena and Reggio Emilia, via Campi 103, 41125 Modena, Italy
[3]Institute of Cancer and Genomic Studies, University of Birmingham, Birmingham B15 2TT, UK
[4]Department of Biochemistry, University of Alberta, Edmonton, Alberta T6G 2H7, Canada
[5]Lead Contact
*Correspondence: fanelli@unimo.it
http://dx.doi.org/10.1016/j.chembiol.2016.07.015

SUMMARY

Uncontrolled activation of Rho signaling by RhoGEFs, in particular AKAP13 (Lbc) and its close homologs, is implicated in a number of human tumors with poor prognosis and resistance to therapy. Structure predictions and alanine scanning mutagenesis of Lbc identified a circumscribed hot region for RhoA recognition and activation. Virtual screening targeting that region led to the discovery of an inhibitor of Lbc-RhoA interaction inside cells. By interacting with the DH domain, the compound inhibits the catalytic activity of Lbc, halts cellular responses to activation of oncogenic Lbc pathways, and reverses a number of prostate cancer cell phenotypes such as proliferation, migration, and invasiveness. This study provides insights into the structural determinants of Lbc-RhoA recognition. This is a successful example of structure-based discovery of a small protein-protein interaction inhibitor able to halt oncogenic Rho signaling in cancer cells with therapeutic implications.

INTRODUCTION

A main family of the Ras superfamily of small GTPases comprises Rho (Ras homolog) proteins (Jaffe and Hall, 2005; Colicelli, 2004). They function as bimolecular switches by adopting different conformational states in response to binding GDP or GTP. Rho activity is promoted by guanine nucleotide-exchange factors (GEFs), which catalyze the exchange of GDP for GTP in vivo.

Most of the RhoGEFs, which comprise 74 distinct members in humans, share a catalytic domain homologous to that of the Dbl oncoprotein (DH domain) (Jaiswal et al., 2013). In most Dbl family GEFs, the DH domain is positioned immediately N-terminal to a pleckstrin homology (PH) domain (Figures 1 and S1) (Rossman et al., 2005).

Rho GTPases and RhoGEFs play important roles in many aspects of cancer development and tumor progression (Karlsson et al., 2009; Cook et al., 2013; Wirtenberger et al., 2006; Feher et al., 2012). In this respect, the oncogenic function of the RhoGEF A-Kinase Anchoring Protein-Lbc (AKAP-Lbc [or AKAP13], hereinafter referred to as Lbc) was discovered a number of years ago (Toksoz and Williams, 1994). Since then, several lines of evidence have shed new light on the potential role of Lbc in the process of tumor development (Lewis et al., 2005; Sterpetti et al., 2006; Wirtenberger et al., 2006; Raponi et al., 2007; Bonuccelli et al., 2009; Hu et al., 2010; Rolland et al., 2010; Feher et al., 2012). Incidentally, Lbc and its close homologs, Leukemia-associated RhoGEF (LARG), p115-RhoGEF (p115), p190-RhoGEF (p190), and PDZ-RhoGEF (PRG), activate RhoA, RhoB, and RhoC but not Rac and Cdc42 (Arthur et al., 2002; Diviani et al., 2001; Jaiswal et al., 2011; Zheng et al., 1995; Jaiswal et al., 2013). Lbc, LARG, p115, and PRG are directly regulated by activated $G\alpha_{12/13}$ proteins (i.e., only $G\alpha_{12}$ in the case of Lbc) and are suggested to play a role in oncogenic transformations induced by G protein-coupled receptors (Diviani et al., 2001;Fukuhara et al., 1999, 2000; Hart et al., 1998; Aittaleb et al., 2009).

Despite its centrality in cancer, the Rho-RhoGEF system has been targeted by a limited number of studies aimed at discovering therapeutic agents (Gao et al., 2004; Bouquier et al., 2009a, 2009b; Vives et al., 2011; Shang et al., 2012; Friesland et al., 2013; Shang et al., 2013; Cardama et al., 2014; Evelyn et al., 2014; Brown et al., 2014).

The main goal of this study was to suppress the oncogenic signals of Lbc by means of small molecules that could impair the ability of the RhoGEF to bind and activate RhoA (i.e., protein-protein interaction [PPI] inhibitors). When the docking experiments were originally performed, no crystallographic structure was available for the DH-PH tandem domain of Lbc. Therefore, a structural model of the Lbc-RhoA complex was predicted based upon the significant sequence similarity with the LARG-RhoA system.

The combination of structural analysis and in vitro alanine scanning mutagenesis, as well as assays for detecting PPI and functionality, identified a circumscribed likely region for RhoA recognition and activation by Lbc. That region was targeted by virtual screening of compound libraries.

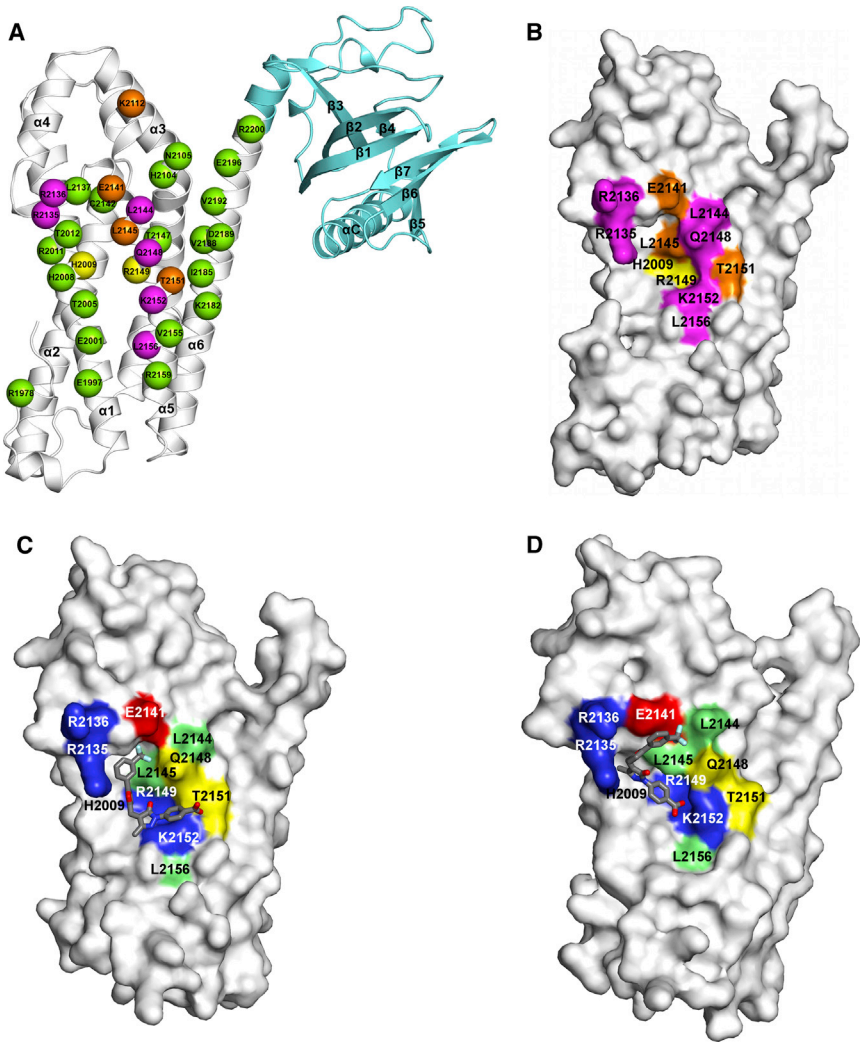

Figure 1. Representations of the Structural Models of Lbc

(A) Cartoons of the predicted structure of Lbc are shown. The DH domain of Lbc is characterized by six α helices organized in an up-down bundle architecture, whereas the PH domain holds a roll architecture made of seven antiparallel β strands (Figures 1A and S1). The spheres centered on the Cα carbons in the DH domain indicate the amino acids that have been targeted by in vitro alanine scanning mutagenesis. Spheres are colored according to the functional consequence of mutation. In detail, magenta and orange colors indicate the amino acids whose alanine replacement results, respectively, in dramatic and moderate impairment in RhoA interaction as well as in dramatic impairment in GEF activity. Those Lbc amino acids that are not essential for RhoA recognition and activation are green; those amino acids that are not essential for interaction with RhoA but relevant for the GEF activity of Lbc are yellow. The PH domain is aquamarine.

(B) The molecular surface of the structural model of Lbc is shown by employing the same view and color coding as in (A). Only those amino acids essential for Lbc-RhoA recognition and/or activation, i.e., functionally relevant, are colored.

(C) The molecular surface of the DH domain of Lbc is shown, starting from the beginning of α1 (i.e., K1990) and ending to α6 (E2203); to put focus on the target region, the α2/α3 loop has been hidden. Only the functionally relevant amino acids inferred from alanine scanning mutagenesis are highlighted, colored according to their polarity. Blue, red, yellow, and light green stand for cationic, anionic, polar, and hydrophobic, respectively. The predicted docking mode of compound A13 is shown. A13 is represented as sticks colored by atom type.

(D) The same graphical representation as in (C) is shown but concerning the predicted docking mode between the A13 lead and the crystal structure of unbound Lbc (PDB: 4D0O). Such docking mode has been obtained by using the same setup as that used for virtual screening, hence setting the flexibility of the K2152 side chain.

See also Table S1, Figures 1 and S5.

We succeeded in discovering a small PPI inhibitor that was able to halt oncogenic Rho signaling pathways in cancer cells with therapeutic implications.

RESULTS

A Circumscribed Region of Lbc Holds the Determinants for RhoA Recognition and Activation

In the predicted Lbc-RhoA complex, almost the totality of the Lbc surface buried by RhoA (i.e., 94.3%) belongs to the DH domain and involves α1, α3, α4/α5 loop, α5, and α6. The interface between Lbc and RhoA highlights the electrostatic complementarity between the two proteins mostly mediated by the following salt bridges: $K2116^{Lbc}$-$D76^{RhoA}$, $R2135^{Lbc}$-$E40^{RhoA}$, $R2136^{Lbc}$-$D45^{RhoA}$, $R2136^{Lbc}$-$E54^{RhoA}$, $E2145^{Lbc}$-$R5^{RhoA}$, $K2152^{Lbc}$-$D59^{RhoA}$, and $E2200^{Lbc}$-$R68^{RhoA}$. The hydrophobic core at the Lbc-RhoA interface is contributed in part by L2144, L2145, and L2156 from Lbc; L2144 and L2145 participate in the binding pocket of W58, an amino acid located in the inter-switch of RhoA that we have found to be essential for Lbc-RhoA interaction (Figure S2). This binding pocket is known as the W58 cage, with Q2148 also contributing to this feature here.

Collectively, our structural model suggested that the main actors in Lbc-RhoA recognition are limited regions of the two proteins, i.e., the α4/α5 loop and the N-terminal half of α5, from Lbc, and switch I (swI) and inter-switch from RhoA. Structure predictions of the complex were supported by in vitro alanine scanning mutagenesis targeting 33 amino acids from α1, α3, α4/α5 loop, α5, and α6, which represent 86% of the DH surface buried by RhoA (Table S1). In vitro experiments were performed by using the isolated GEF module of Lbc, which displays constitutive RhoGEF activity (Baisamy et al., 2005; Diviani et al., 2001, 2004).

To initially assess the impact of the different mutations on the ability of Lbc to bind RhoA, pull-down experiments were performed by incubating extracts of HEK293 cells overexpressing wild-type or mutated Flag-tagged Lbc constructs with purified

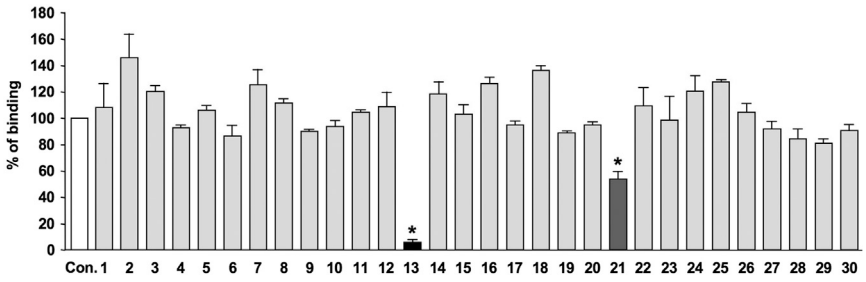

Figure 2. Compounds A13 and A21 Inhibit Lbc-RhoA Interaction

HEK293 cells expressing Flag-tagged Lbc were serum starved for 24 hr and lysed. Cell extracts were incubated with glutathione Sepharose beads coupled to GST-tagged RhoA in the presence of 1% DMSO (control) or 100 μM of 30 compounds identified by virtual screening and shown in Table S2. The relative levels of Flag-Lbc associated with GST-RhoA were detected by western blot and quantified by densitometry. Results are the mean ± SE of three to eight independent experiments. *$p < 0.05$ compared with the amount of Flag-Lbc bound to GST-RhoA under control conditions. See also Table S2.

GST-tagged RhoA. Mutations of K2112, E2141, L2145, and T2151 reduced the interaction between Lbc and RhoA by about 30%–50% (Figures S3C–S3F; colored orange in Figures 1 and S1), whereas mutations of R2135, R2136, L2144, Q2148, K2152, and L2156 reduced the ability of Lbc to bind RhoA up to 90% (Figures S3E and S3F; colored magenta in Figures 1 and S1). In contrast, binding was mildly or not affected by mutations within αN1, α1, α3, and α6 (Figures S3A, S3B, S3G, and S3H; colored green in Figures 1 and S1). Indeed, no binding was observed between the different Flag-tagged Lbc constructs and GST alone (data not shown).

The impact of Lbc mutations on the GEF activity inside cells was determined by the Rhotekin capture assay. As shown previously (Diviani et al., 2001, 2004), overexpression of Flag-Lbc promoted a significant increase in RhoA-GTP formation compared with mock transfected cells (Figures S4A, S4C, S4E, and S4F, upper panel, lane 2). In line with mutational effects on Lbc-RhoA interaction presented above, alanine substitutions for K2112 R2135, R2136, E2141, L2144, L2145, Q2148, T2151, K2152, and L2156 significantly inhibited the ability of Lbc to promote RhoA activation inside cells (Figures S4C–S4F). Surprisingly, mutations of H2009 and R2149 (colored yellow in Figures 1 and S1), despite their minor impact on Lbc-RhoA interaction (Figures S3A, S3E, S3B, and S3F), strongly affected Lbc-mediated RhoA activation (Figures S4A, S4E, S4B, and S4F). This suggests that these residues might selectively participate in the guanine nucleotide-exchange reaction leading to RhoA activation.

Collectively, the combination of structural analysis of the predicted Lbc-RhoA complex, in vitro alanine scanning mutagenesis, and assays for detecting PPI and functionality identified a limited region of Lbc as responsible for recognizing and/or activating RhoA (Figure 1B).

Structure-Based Discovery of PPI Inhibitors Targeting Lbc

Consistent with structure predictions and determinations, the 12 amino acids relevant for RhoA recognition and/or activation by Lbc circumscribe a region representing 38% of the DH surface buried by RhoA (Figure 1).

This region of Lbc, comprising the N-terminal halves of α1 and α5 and the α4/α5 loop, was targeted by virtual screening aimed at finding small molecules able to compete with RhoA in interacting with Lbc. The electrostatic features of the target region of Lbc, i.e., enriched in cationic amino acids, were exploited to restrict the compound library to only anionic species. This allowed us to reduce by almost 17-fold the over 15 million compounds downloaded from the Zinc database (http://zinc.docking.org). Minimization of the structural redundancy of the 850,000 screened compounds, paired with filtering according to docking score and number of ligand contacts with the hot region, ultimately served to further reduce the number of considered compounds by over 1,100-fold. This process led to selection of 30 compounds for in vitro testing (Table S2). Those compounds are structurally dissimilar from each other with the exception of compounds A07 and A10, selected for their docking score, as well as A13 and A29, which share only a common fragment.

GST pull-down experiments using cell lysates determined the ability of those compounds to inhibit the interaction between Lbc and RhoA. Two compounds, A13 and A21, resulted in an inhibition higher than 90% and equal to 43%, respectively, of the binding of Lbc to GST-RhoA (Figure 2). As for A13, the full PPI inhibitor, according to the predicted docking mode, both the benzoate and pyrazole moieties interact with the K2152 hotspot (see the Markush structure in Table 1). The phenyl substituent on the furane ring docks into a cavity formed by T2005, L2137, and L2145; the latter, which participates in the W58 cage, interacts with the trifluoro-methyl group (R5 substituent in Table 1, and Figure 1).

The crystallographic structures of free (PDB: 4D0O) and RhoA-bound (PDB: 4D0N) Lbc released when our study was completed (Abdul Azeez et al., 2014), provided further validation to our structure predictions (see Supplemental Information and Figures S5A–S5C).

To gain insights into the interaction mode of A13, we docked the compound into the crystal structure of free Lbc using a setup identical to that used for virtual screening. The predicted docking pose is slightly shifted compared with the one in the Lbc model due, at least in part, to a slight change in the cavity that accommodates the trifluoro-methyl-substituted phenyl ring and to a different conformation of K2152 (Figures 1C and 1D). The two docking modes share the salt bridge between the carboxylate of the ligand and the hotspot K2152 as well as the interaction between the trifluoro-methyl-group of the ligand and the hotspot L2145. In the new docking mode, these two portions of the ligand make additional interactions with the hotspots R2149 and L2146, respectively. Remarkably, the trifluoro-methyl group of the ligand docks into the W58 cage, an important recognition site for the G protein (Figures 1C and 1D). Changing

Table 1. Effects of the A13 Analogs on Lbc-RhoA Interaction

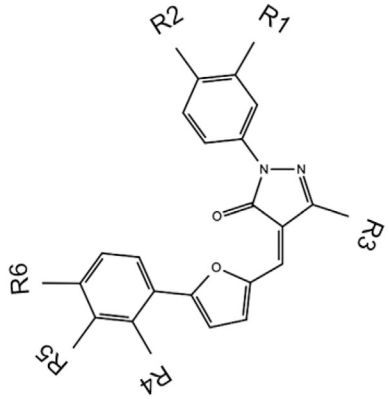

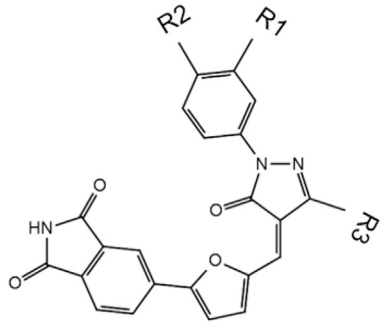

A32

ID	R1	R2	R3	R4	R5	R6	% Lbc[a]	IC_{50Lbc}[b]
A13	H	COO^-	CH_3	H	CF_3	H	6.02 ± 0.67	3.6 ± 1.3
A31	H	COO^-	CH_3	NO_2	H	OCH_3	64.37 ± 27.34	
A32	H	COO^-	CF_3				40.78 ± 15.65	
A33	H	COO^-	CF_3	H	H	COO^-	20.95 ± 3.71	15.4 ± 1.7
A34	H	COO^-	CH_3	NO_2	H	CH3	62.70 ± 13.65	
A35	H	COO^-	CH_3	H	H	SO_2NH_2	44.88 ± 8.62	
A36	H	COO^-	CH_3	H	H	$COOCH(CH_3)_2$	33.28 ± 6.25	
A37	H	COO^-	CH_3	H	H	Cl	50.71 ± 18.61	
A38	H	COO^-	CH_3	H	$COOC_2H_5$	Cl	19.09 ± 3.74	20.1 ± 1.9
A39	H	COO^-	CF_3	H	NO_2	H	46.17 ± 9.66	
A40	H	COO^-	CF_3	H	$COOCH_3$	H	24.59 ± 12.91	8.2 ± 1.4
A41	H	COO^-	CH_3	CH_3	Cl	H	61.15 ± 9.96	
A42	H	COO^-	CH_3	Br	H	H	43.13 ± 13.80	
A43	H	COO^-	CH_3	F	H	H	16.33 ± 4.10	9.2 ± 1.6
A44	H	SO_2NH_2	CH_3	H	COO^-	H	51.11 ± 11.47	
A45	COO^-	H	CH_3	H	CF_3	H	12.26 ± 2.40	10.9 ± 1.9
A46	COO^-	H	CH_3	H	$COOCH_3$	H	19.36 ± 4.15	29.0 ± 4.3
A47	COO^-	H	CH_3	H	COO^-	H	47.98 ± 8.50	
A48	COO^-	H	CF_3	H	COO^-	H	39.83 ± 10.80	
A49	CF_3	H	CH_3	H	COO^-	H	113.07 ± 6.07	
A50	H	H	CH_3	H	H	COO^-	72.18 ± 7.19	

See also Table S3 and Figure S11.

[a]% of Lbc-RhoA binding in the presence of the compound; results are the mean ± SE of three to four independent experiments.

[b]IC_{50} (μM) relative to the ability to inhibit the interaction between RhoA and Lbc; results are the mean ± SE of three independent experiments.

computational conditions, i.e., by assigning an alternative rotamer to R2136 and introducing the additional flexibility of R2135, did not change the best docking pose, while slightly improving the score. Incidentally, docking in a rigid-side chain mode also does not change the best docking pose, while lowering the docking score.

To further validate the predicted docking mode into the crystal structure, A13 was also docked onto the 75,000 frames constituting a 0.75 μs molecular dynamics (MD) trajectory of unbound Lbc in explicit solvent (see Supplemental Information). Docking solutions tend to group into six major clusters, one of which resembles the predicted docking mode. MD relaxation (10 ns) of the best scored (the orientation of A13 in that complex is shown in Figure S5D, colored magenta) and the center complexes from each of the six clusters shows that the predicted docking mode is more stable than the others (see Supplemental Information). To further validate such docking mode, the last frame of the relaxed trajectory from the best scored solution was subjected to 60 ns of adaptive temperature MD (Zhang and Ma, 2010). Cluster analysis on the 1,637 frames corresponding to a temperature range 300–305 K over the last 40 ns served to identify the most populated cluster whose center is shown in Figure S5D. The average A13 root-mean-square deviation (RMSD) between the frames of the whole trajectory and the input structure of MD relaxation was 2.18 ± 0.70 Å. Such RMSD was computed following the superimposition of all heavy atoms of A13 and the 1,993–2,168 atom range of LbcDH.

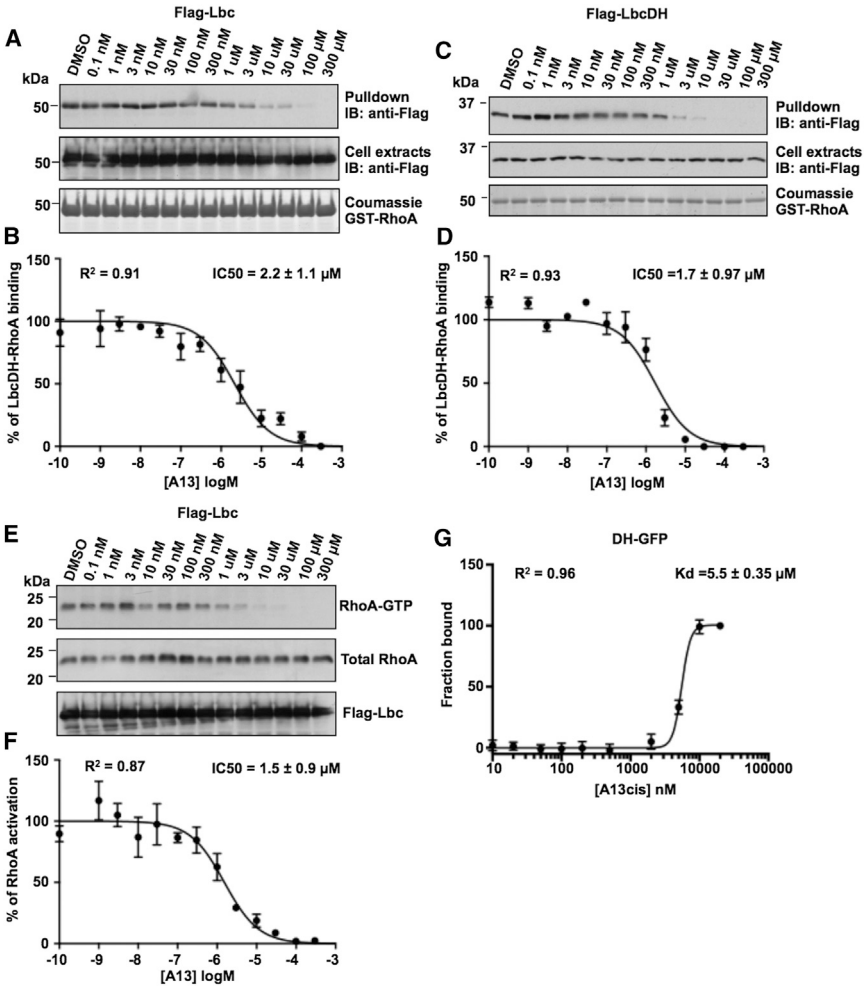

Figure 3. Compound A13 Inhibits Lbc-Mediated RhoA Activation through Direct Interaction with the DH Domain

(A and C) HEK293 cells expressing Flag-Lbc (A) or Flag-LbcDH (C) were serum starved for 24 hr and lysed. Cell extracts were incubated with glutathione Sepharose beads coupled to GST-tagged RhoA in the presence of DMSO or increasing concentrations of A13. The relative levels of Flag-Lbc or Flag-DH associated with GST-RhoA (upper panels) and expressed in cell extracts (middle panels) were detected by western blot using anti-Flag monoclonal antibodies. A control protein staining indicating the amounts of GST-RhoA used in the pull-down assay is shown (lower panels).

(B and D) Quantitative analysis of Flag-Lbc or Flag-LbcDH associated with the GST-RhoA was obtained by densitometry. Results are the means ± SE of three independent experiments.

(E) HEK293 cells transfected with empty pFlag vector or plasmid encoding Flag-tagged Lbc were serum starved for 24 hr in the presence of increasing concentrations of A13. GTP-bound RhoA was affinity purified from cell extracts using glutathione Sepharose beads coupled to GST-RBD. The bound RhoA was detected with a monoclonal anti-RhoA antibody (upper panel). The relative amounts of total RhoA and Flag-Lbc proteins in the cell lysates were assessed using monoclonal antibodies against RhoA (middle panel) and Flag (lower panel), respectively.

(F) Quantitative analysis of the GTP-RhoA associated with RBD beads was obtained by densitometry. Values were normalized to the RhoA and Flag-Lbc content of cell extracts. Results are expressed as means ± SE of three independent experiments.

(G) Microscale thermophoresis analysis of the interaction between A13cis and DH-GFP. Purified DH-GFP (25 nM) was incubated with increasing concentrations of A13 (1 nM–20 µM). The fraction of bound DH-GFP is plotted as a function of [A13cis]. Results are the means ± SE of three independent experiments.

See also Figures S6–S10.

Collectively, the convergence of a number of docking and MD simulations corroborates the predicted interaction mode of the PPI inhibitor.

A13 Inhibits Lbc-RhoA Interaction and the GEF Activity of Lbc by Binding to the DH Domain

The effectiveness of A13 in inhibiting the interaction between the DH domain of Lbc (LbcDH) and RhoA as well as the ability of Lbc to activate RhoA in intact cells was evaluated over a concentration range from 1 pM to 300 µM, using GST pull-down and Rhotekin capture assays, respectively (Figures 3A–3E).

Binding of RhoA to Lbc and LbcDH was inhibited at 2.2 µM and 1.7 µM half maximal inhibitory concentration (IC_{50}), respectively (Figures 3A–3D), whereas Lbc-induced RhoA-GTP formation was inhibited at 1.5 µM IC_{50} (Figures 3E and 3F). These results indicate that A13 can cross the plasma membrane barrier to efficiently inhibit Lbc inside cells.

The binding constant of A13 to Lbc was measured as well by microscale thermophoresis, which allows sensitive and quantitative analysis of the interaction between small molecules and proteins. Cell lysates expressing GFP or GFP-tagged Lbc were incubated with concentrations of A13 ranging from 1 nM to 20 µM. The analysis indicated that A13 binds Lbc-GFP with a dissociation constant (K_d) of 1.6 µM (Figure S6A), which is in line with the IC_{50} values (Figure 3B). No binding was detected between A13 and GFP (Figure S6A). The tested compound is a 50% mixture of *cis* and *trans* isomers concerning the relative positions of the methyl group and the olefinic proton (i.e., the *cis* conformer corresponds to the Markush structures in Table 1). An ad hoc synthesized mixture enriched in the *cis* isomer (i.e., A13cis, *cis*:*trans* 75:25) bound Lbc-GFP with a K_d of 0.9 µM (Figure S6B), thus suggesting that the *cis* isomer might display higher affinity for Lbc than the *trans* isomer. This result is consistent with A13 holding a *cis* configuration in all predicted docking poses (Figures 1C, 1D, and S5D).

Direct interaction between A13cis and the DH domain of Lbc was demonstrated by microscale thermophoresis experiments, which showed that A13cis bound the purified GFP-tagged LbcDH domain (LbcDH-GFP) with a K_d of 5.5 µM (Figure 3G).

Measurement of the in vitro affinity of A13cis was also carried out by other biophysical techniques. Several methods were probed to circumvent the problem associated with the solution state of A13cis. The buffer conditions were improved by solubilizing the compound in DMSO (up to 10%) and supplementing the solution with detergent. The specificity of the binding was confirmed by surface plasmon resonance (SPR) detection experiments that showed that A13cis bound Lbc with a K_d of 6.3 μM (Figure S7A), whereas no significant binding could be detected for the PH domain (K_d >50 μM, Figure S7B, Supplemental Experimental Procedures).

Consistent with K_d determinations by both microscale thermophoresis and SPR, A13cis exerts inhibition of the guanine nucleotide-exchange reaction catalyzed by LbcDH (Figures S8A and S8B, and Supplemental Experimental Procedures).

Collectively, we found that A13 inhibits LbcDH-RhoA interaction in a dose-dependent manner in vitro, and the Lbc-induced RhoA activation in intact cells.

The A13 Lead Acts as a PPI Inhibitor also for LARG and PRG, p114, p190, and GEFH1 but Not p115, p63, and Net1

The selectivity of A13 in inhibiting the interaction between RhoA and RhoGEFs of the Lbc subfamily was assessed by using GST pull-down assays. Extracts of HEK293 cells overexpressing Flag-tagged Lbc, LARG, PRG, and p115 were incubated with purified GST-tagged RhoA in the absence or presence of 100 μM of A13. In addition to inhibiting the RhoA-Lbc interaction, the compound could also inhibit the interaction of RhoA with LARG and PRG at 4.2 μM and 11.4 μM IC_{50}, respectively (Figure S9). In contrast, A13 did not affect the binding between RhoA and p115 (Figure S9). To further investigate the selectivity of A13 toward RhoGEFs, we assessed the ability of the compound to inhibit RhoA activation induced by LARG, p114, p190, GEFH1, PRG, p115, p63, and Net-1. We found that A13 inhibits LARG-, p190-, p114-, GEFH1-, and PRG-mediated RhoA activation at 1.9 μM, 4.6 μM, 5.8 μM, 8.8 μM, and 14.6 μM IC_{50}, respectively, without affecting the activity of p115, p63, and Net-1 (Figure S10). These data indicate that A13 is effective only on Lbc and its closest homologs LARG-, p190-, p114-, GEFH1-, and PRG, which is indicative of some selectivity.

Insights from Structure-Activity Relationship Analysis

In an attempt to infer structure-activity relationships (SAR), we also determined the ability of 20 commercially available close analogs of A13 to inhibit the Lbc-RhoA interaction in vitro (Table 1 and Figure S11).

Almost all the selected compounds except for A31, A34, and A41 (sharing a bulky R4 substituent) as well as compounds A49 and A50 (lacking the R1 or R2 carboxylate, respectively) inhibit Lbc-RhoA binding by ≥45% (Table 1 and Figure S11). Among them, six compounds, i.e., A33, A38, A40, A43, A45, and A46, inhibit Lbc-RhoA binding by ≥75% at IC concentrations in the low micromolar range (Table 1 and Figure S11). Remarkably, the six active compounds, similar to A13, can inhibit RhoA binding to LARG and PRG but not to p115 (Table S3).

SAR analysis clearly emphasizes the importance of the carboxylate group at R1 or, better, at R2 for the PPI inhibitory activity. As for R3, SAR analysis is not informative because commercially available analogs worth testing hold only $–CF_3$ or $–CH_3$ as R3. Bulky R4 substituents do not appear to be tolerated, while lipophilic or weakly polar R5 substitutions are preferred to polar or charged groups. Incidentally, a close analog of the inactive compound A34, differing from A34 in the presence of a $–CH_3$ in *para* to the $–NO_2$ group, has been found to inhibit p300/CBP histone acetyltransferase (Bowers et al., 2010). As for the R6 substituent, the main information that emerges from SAR analysis is that when R4 and R5 are unsubstituted, a negatively charged group favors PPI inhibition more than neutral and lipophilic substituents.

Collectively, SAR analysis strengthens the supposition that a carboxylate group in the right position is essential for significant PPI inhibition, while certain substituents in specific positions disfavor such inhibition.

A13 Shoots down Cellular Responses Induced by the Lbc-RhoA Pathway and Significantly Reduces the Malignant Properties of Prostate Cancer Cells

Preliminary SAR analysis strengthens the case for A13 as a lead compound. We therefore tested a number of cellular responses to A13 treatment. To examine the inhibitory action of such compound on the cellular responses promoted by the Lbc-RhoA pathway, we first measured the effect of A13 treatment on the ability of Lbc to induce the formation of actin stress fibers in NIH3T3 fibroblasts. As previously shown (Diviani et al., 2001), Rho-selective GEFs promote formation of actin stress fibers in fibroblasts (Figure 4A). Interestingly, A13 treatment completely abolishes these effects, proving that it can efficiently inhibit the ability of Lbc to induce reorganization of the actin cytoskeleton. This effect is likely to be the consequence of direct GEF inhibition since A13 does not interfere with actin stress fiber formation induced by the overexpression of the constitutively active RhoA Q63L mutant (Figure 4B). Likewise, A13 inhibits stress fiber formation induced by selected Lbc homologs including LARG, p190, p114 without affecting cytoskeletal reorganization induced by p115, p63, and Net1 (Figure 4A).

Since Lbc induces cell transformation by activating RhoA, we further determined if A13 was able to inhibit Lbc-induced transformation of NIH-3T3 fibroblasts. Indeed, A13 treatment of Flag-tagged Lbc-overexpressing cells reduced their foci-forming potential by 70% (Figures 4C and 4D).

It is well recognized that overactivation of RhoA signaling plays a prominent role in the pathogenesis of prostate cancer (Schmidt et al., 2012). Recent studies performed on the highly invasive PC-3 prostate cancer cells have shown that RhoA activation contributes to the enhanced migratory and invasive properties of this cell line (Zhang et al., 2013; Hodge et al., 2003). Interestingly, PC-3 cells express AKAP13, LARG, and PRG, which have been proposed to mediate signals associated with prostate cancer cell proliferation, migration, and invasion (Lewis et al., 2005; Wang et al., 2004).

Based on these observations, we initially assessed, by the Rhotekin RBD or PAK1-CRIB pull-down assays, if A13 could affect the activity of RhoA, RhoB, RhoC, Rac1, and Cdc42 in PC-3 prostate cancer cells (Figure 5). Our results indicate that incubation of PC-3 prostate cancer cells with 10 μM of A13 inhibits

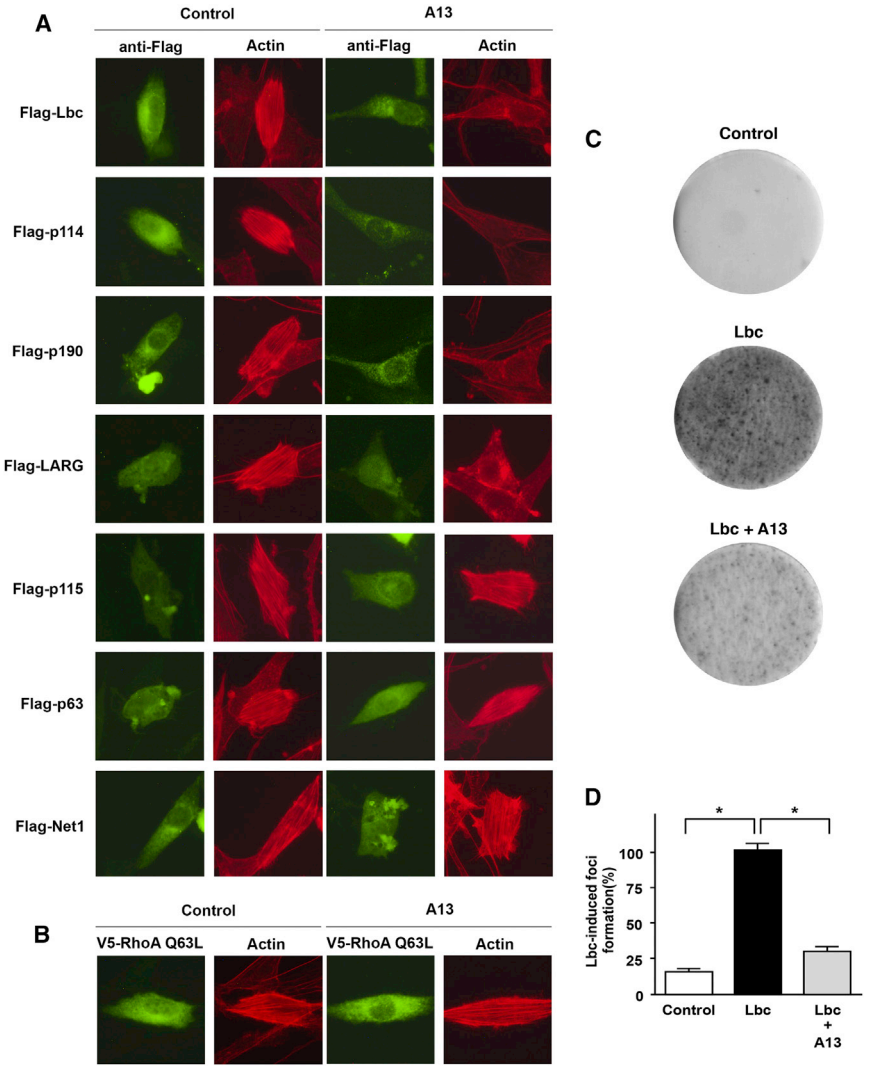

Figure 4. Inhibition of the Ability of Lbc to Induce Stress Fiber Formation and Cell Transformation in NIH-3T3 Fibroblasts using Compound A13

(A and B) NIH-3T3 fibroblasts were transfected with the cDNAs encoding Flag-tagged DH-PH tandem domains of various RhoGEFs (A) or V5-RhoA Q63L (B). Transfected cells were serum starved for 24 hr in the absence or presence of 10 μM (A) or 100 μM (B) of A13 and subsequently fixed and permeabilized. The expression of the different Flag-tagged DH-PH constructs and V5-RhoA Q63L was assessed by incubating cells with mouse anti-Flag and anti-V5 antibodies, respectively, followed by fluorescein-isothiocyanate-conjugated donkey anti-mouse secondary antibodies. Actin was detected using Texas red phalloidin.

(C) The results of the focus formation assay of NIH3T3 cells stably transfected with the empty pFlag vector (control) or with the cDNA encoding Flag-Lbc and subsequently treated in the absence or presence of 10 μM A13. Focus formation was evaluated after 21 days of culture.

(D) Quantitation of three independent focus formation assays is shown. Cell transformation induced by Flag-Lbc was set to 100%. Error bars represent SEs. *p < 0.05 compared with the number of foci measured in cells expressing Flag-Lbc.

RhoA by 60% (Figures 5A and 5B) and RhoC by 37% (Figures 5E and 5F), without affecting RhoB (Figures 5C and 5D), Rac1 (Figures 5G and 5H), and Cdc42 (Figures 5I and 5J).

We next assessed the impact of A13 on the proliferative, migratory, and invasive properties of PC-3 prostate cancer cells. Interestingly, we could show that 10 μM of A13 can inhibit cell proliferation by 43% (Figures 6A and 6B), wound healing by 45% (Figures 6C and 6D), random migration by 57% (Figures 6E–6H), and invasiveness by 52% (Figures 6I and 6J).

In control experiments, we could show that the LARG inhibitor Y16 does not affect PC-3 cell proliferation (Figures S12A and S12B), migration (Figures S12C and S12D) and invasion (Figures S12E and S12F). These findings suggest that LARG does not contribute to the oncogenic behavior of PC-3 cells and that the effect of A13 on PC-3 cancer cell properties is not due to the inhibition of LARG.

Importantly, RNAi-mediated knockdown of Lbc in PC-3 cells reduces wound healing by approximately 30%, suggesting that Lbc contributes to the migratory behavior of prostate cancer cells (Figure S13). The fact that the inhibition observed following Lbc silencing (−30%) is slightly weaker compared with that induced by A13 (−45%) could be due to the fact that the knockdown of Lbc is not complete (30% of residual Lbc expression) or that A13 inhibits additional Lbc homologs in PC-3 cells (i.e., p114, p190, GEFH1, or PRG).

Collectively, tests on actin stress fiber and foci formation reveal that A13 inhibits the oncogenic properties of Lbc because of its PPI inhibitory action toward the Lbc-RhoA system. More importantly, A13 is able to significantly reduce the tumorigenic potential of prostate cancer cells likely due to its PPI inhibitory action toward the complex between RhoA (and RhoC although to a significantly lesser extent) and Lbc. Close homologs of Lbc such as p190, p114, GEFH1, and PRG, but not LARG, may also contribute to the effects of A13 on PC-3 cells.

DISCUSSION

Overexpression and genetic variants of the Lbc oncogene (Toksoz and Williams, 1994) have been involved in a number of human tumors (Bonuccelli et al., 2009; Hu et al., 2010; Lewis et al., 2005; Sterpetti et al., 2006; Wirtenberger et al., 2006) and have been shown to correlate with poor cancer prognosis and increased resistance to cancer therapy (Raponi et al., 2007; Rolland et al., 2010). The oncogenic action of Lbc is shared with the close homologous members of the Lbc subfamily, e.g., LARG, PRG, p115, p114, p190, and GEFH1 (Cook et al., 2013; Gu et al., 2006; Hart et al., 1996; Huang et al., 2011; Wang

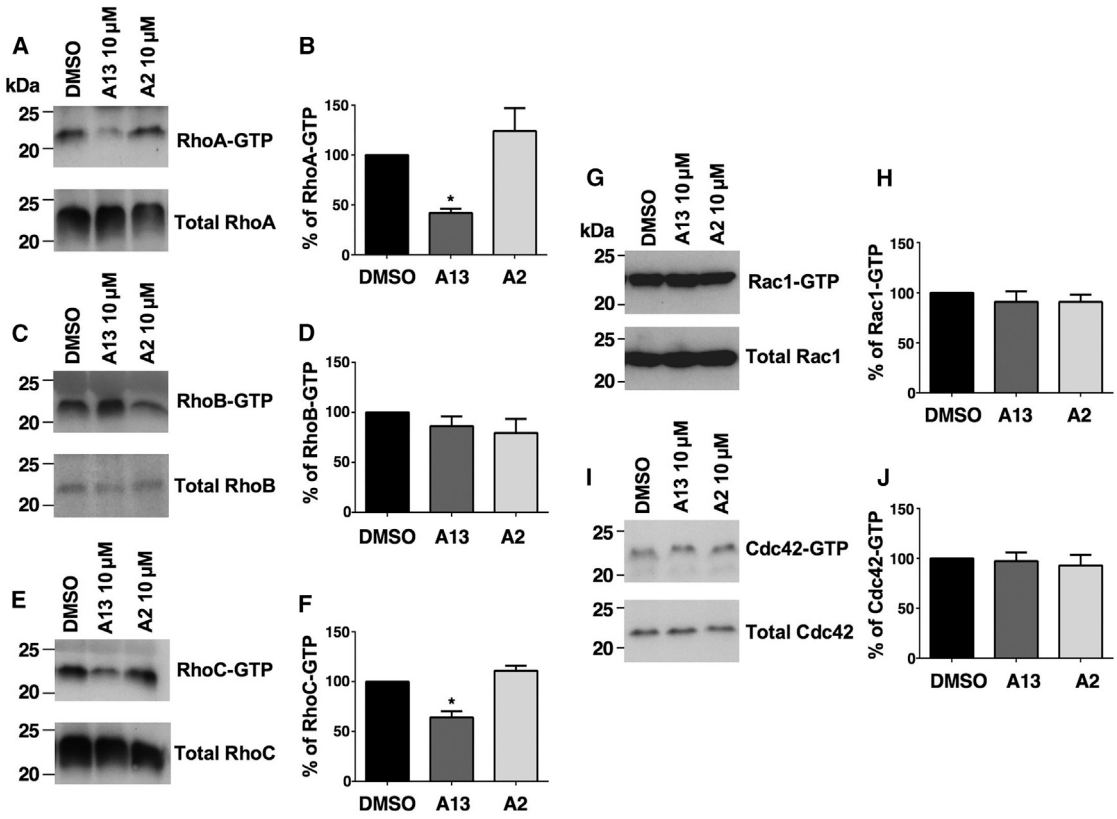

Figure 5. A13 Inhibits Rho Signaling in PC-3 Cells

(A, C, E, G, and I) PC-3 cells were incubated for 24 hr with or without 10 μM A13 or A2. The final DMSO concentration was kept at 1% DMSO. GTP-bound RhoA (A), RhoB (C), RhoC (E), Rac1 (G), and Cdc42 (I) were affinity purified from cell extracts using glutathione Sepharose beads coupled to GST-RBD or GST-CRIB and detected using specific antibodies (upper panels). The relative amounts of total RhoA (A), RhoB (C), RhoC (E), Rac1 (G), and Cdc42 (I) in the cell lysates were assessed by western blot using the indicated antibodies (lower panels).

(B, D, F, H, and J) Quantitative analysis of GTPase activation was obtained by densitometry. The amounts of GTP-bound GTPases were normalized to the GTPase content of cell lysates: RhoA-GTP (B), RhoB-GTP (D), RhoC-GTP (F), Rac1-GTP (H), and Cdc42-GTP (J). Results are expressed as means ± SE of 3–6 experiments. *$p < 0.05$ compared with GTP-bound GTPases levels measured in control cells (DMSO).

et al., 2004). It is worth noting that these close homologous RhoGEFs tend to form supramolecular complexes containing different GEF species potentially able to coordinate and process multiple pro-oncogenic signals in cancer cells (Chikumi et al., 2004). Consistently, a number of findings indicate that cancer cell migration and invasion are regulated by more than a single RhoGEF (Huang et al., 2011; Wang et al., 2004). This suggests that strategies aimed at inhibiting the pro-oncogenic effects of aberrant Rho signaling in cancer cells should rely on the simultaneous inhibition of multiple Lbc subfamily RhoGEFs.

In this study, prediction of the structural complex between Lbc and RhoA was instrumental in driving in vitro experiments to identify the critical surface of Lbc responsible for mediating RhoA recognition and activation. Indeed, we found a circumscribed hot region representing almost 38% of the DH surface buried by RhoA and essentially contributed by the α4/α5 loop and α5, which recognize the swI and inter-switch of the G protein. That region, rich in cationic amino acids, was targeted by virtual screening of small anionic compounds, leading to the discovery of two compounds, A13 and A21, which could inhibit the interaction between Lbc and RhoA in cell lysates by more than 90% and by 43%, respectively.

The biochemical characterization was pursued only for the most active compound, which, in a mixture enriched in *cis* isomer, bound LbcDH with 5.5 μM K_d. The predicted docking mode suggests that the PPI inhibitory action of A13 is due to a competition with RhoA for an LbcDH site comprising K2152 and R2149 hotspots, the W58 cage, and the cavity delimited by the fourth to sixth turns of α1 and the α4/α5 loop. By binding to LbcDH, A13 inhibits the guanine exchange reaction catalyzed by Lbc.

The compound proved able to cross the plasma membrane and inhibit both RhoA recognition and activation by Lbc inside cells in a dose-dependent manner. The demonstrated inhibition of actin stress fiber and foci formation in fibroblasts further strengthened the ability of A13 to block the Lbc-RhoA pathway.

Evidence collected over the past few years suggests that RhoA and its closely related isoforms, RhoB and RhoC, play a crucial role in the pathogenesis of prostate cancer (Muller et al., 2002; Somlyo et al., 2000; Zhang et al., 2013; Ward et al., 2011; Hodge et al., 2003; Senapati et al., 2010). Importantly, PC-3 prostate cancer cells express several Rho-specific GEFs, including Lbc, LARG, PRG, and p115, which have been shown to promote activation of Rho subfamily members (Lewis

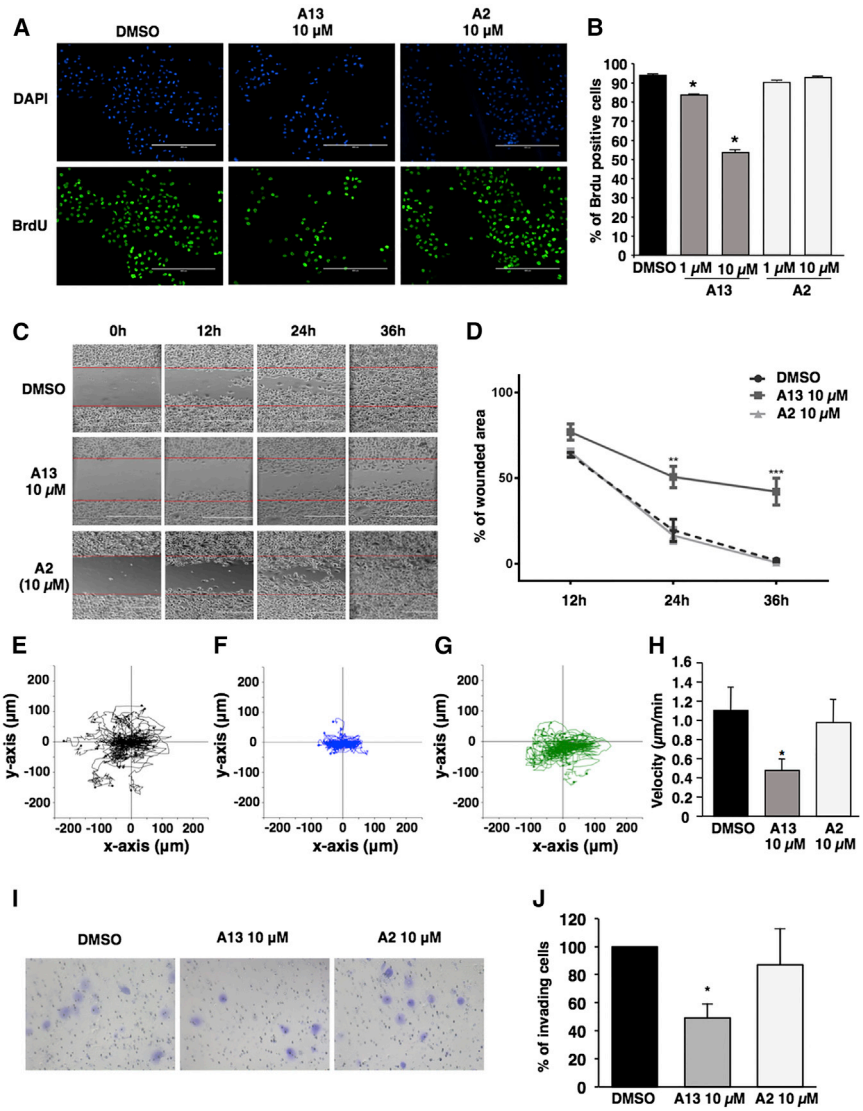

Figure 6. A13 Inhibits Proliferation, Migration, and Invasion of Prostate Cancer Cells

(A) PC-3 cells were incubated for 24 hr with 10% FBS and 10 μM BrdU in the absence or presence of 10 μM A13 or A2. Cells were then fixed, permeabilized, and incubated with DAPI to detect nuclei, and with rat anti-BrdU antibodies as well as Alexa Fluor 488-conjugated anti-rat secondary antibodies to detect proliferating cells. Scale bar, 400 μm.

(B) The percentage of BrdU-positive cells was determined on a total of 2,300–3,000 cells per condition. *$p < 0.05$ compared with the percentage of BrdU-positive cells measured under control conditions.

(C) Wounded PC-3 cells monolayers were cultured for 36 hr in RPMI1640 supplemented with 10% FBS in the absence or presence of 10 μM A13 or A2. Recolonization of the wounded area was imaged every 12 hr. Scale bar, 1,000 μm.

(D) Quantitation of the wound-healing process. **$p < 0.01$, ***$p < 0.001$ compared with the wounded area measured under control conditions.

(E–H) PC-3 cells were grown in RPMI1640 supplemented with 10% FBS and incubated in the absence or presence of 10 μM A13 or A2. Random migration was imaged using time-lapse microscopy for a period of 10 hr. Migration trajectories (E–G) and velocities (μm/min) (H) were determined on a total of 160 cells per condition. (H) *$p < 0.05$ compared with the migration velocity measured under control conditions.

(I) PC-3 cells (2.5×10^4) were seeded on Matrigel-coated transwell membranes with 8 μm pores and cultured for 36 hr in RPMI1640 supplemented with 10% FBS in the absence or presence of 10 μM A13 or A2. Membranes were fixed, and cells migrated on the underside of the membrane were visualized using 2% crystal violet. Representative fields for each condition are shown.

(J) The percentage of invading cells was determined on three transwell membranes per condition. *$p < 0.05$ compared with the percentage of invading cells measured under control conditions.

et al., 2005; Wang et al., 2004). In line with these findings, our functional studies now demonstrate that A13 can reduce RhoA and, to a significantly lesser extent, RhoC, but not RhoB activation in PC-3 prostate cancer cells.

The findings that A13 inhibits Lbc and its closest homologs LARG, PRG, p190, p114, and GEFH1 without influencing the activity of p115, p63, Net-1 suggests that it exerts a preferential PPI inhibitory action toward a subgroup of Lbc-subfamily GEFs. Moreover, the fact that A13 does not affect Rac1 or Cdc42 activation suggests that the compound does not inhibit the activity of Rac or Cdc42 activating GEFs expressed in PC-3 cells. Importantly, the compound efficiently reverses a number of PC-3 prostate cancer cell phenotypes including proliferation, migration, and invasiveness. The finding that A13 is significantly less effective following partial silencing of Lbc in PC-3 cells suggests that the antitumoral properties of A13 on those cells are indeed mediated by Lbc.

The first virtual screening study targeting a RhoGEF led to the discovery of an inhibitor of the LARG-RhoA interaction, Y16, which was not active on Lbc and displayed antitumoral activity (Shang et al., 2013). Remarkably, our findings that Y16 is not active against PC-3 cells together with the results of Lbc silencing and of the other experiments done in this study indicate that the antitumoral effects of A13 on those cells indeed involve Lbc and probably some other Lbc subfamily RhoGEF but not LARG and p115.

We filed a patent on A13 as an inhibitor of the Lbc-RhoA interaction with therapeutic potential in cancer (patent no. MI2013A001410 deposited on August 26, 2013, and published as WO2015/028929A1). A patent published in 2014 (EP 2 682 118 A1) reports on psoralen derivatives for the treatment of heart failure and heart hypertrophy via inhibition of the Lbc-RhoA interaction. This compound, 3-(4-methoxyphenyl)-5,6-dimethyl-furo [3,2-g]chromen-7-one, is structurally unrelated and less active (i.e., IC_{50} = 25.9 μM) than the A13 compound reported here. Importantly, the discovery of the psoralen compound did not arise from structure-based virtual screening, which makes its optimization more difficult. The first structure-based discovery

of the Lbc-RhoA interaction inhibitor presented here offers a step forward toward lead optimization aimed at improving solubility, affinity, and specificity.

SIGNIFICANCE

The study provides significant insights into the structural determinants of Lbc-RhoA recognition, a process with central implications in cancer biology. Indeed, we found that a circumscribed positively charged region of the RhoGEF can be targeted by small anionic molecules to impede RhoA binding and, consequently, the activation of oncogenic Rho signaling pathways in cancer cells.

The study also contributes to expand the yet too small chemical space spanned by small PPI inhibitors, which are difficult to discover. Meeting the challenge relied on a computational strategy based strictly on the predicted structural features of the target protein both in setting the compound library and the virtual screening input as well as in filtering the hit compounds from the screening. Such a rational approach succeeded in finding a chemical scaffold able to halt the oncogenic properties of Lbc by inhibiting Lbc-RhoA interaction inside cells. Remarkably, the lead compound, A13, also holds anti-tumorigenic potential, being able to reverse a number of prostate cancer cell phenotypes.

The PPI inhibitory action of such compound is likely due to a competition with RhoA for an LbcDH binding site comprising the K2152 and R2149 hotspots, the W58 cage, and the cavity delimited by the fourth to sixth turns of α1 and the α4/α5 loop. The compound acts as a PPI inhibitor also for other RhoGEFs such as LARG, PRG, p190, p114, and GEFH1 but not p115, p63, and Net-1, indicative of some selectivity. The antitumoral properties of A13 on PC-3 prostate cancer cells are mediated by Lbc and probably some other close homologs but not LARG and p115.

Ultimately, our results strengthen the evidence that targeting Lbc subfamily RhoGEFs might emerge as a promising strategy for new therapeutic approaches aimed at inhibiting tumor progression and metastasis.

EXPERIMENTAL PROCEDURES

In Silico Experiments: Comparative Modeling

The structural model of the DH-PH tandem domain of Lbc in complex with RhoA was built by comparative modeling (by means of MODELLER; Sali and Blundell, 1993), using the crystal structure of the LARG-RhoA complex as a template (PDB: 1X86) (Kristelly et al., 2004). Further details on comparative modeling can be found in the Supplemental Information.

In Silico Experiments: Virtual Screening

Virtual screening was carried out by means of AutoDock Vina 1.1.1 (Trott and Olson, 2010). The docked library comprised an ensemble of 850,000 negatively charged compounds from the Drug-like, Lead-like, NCI-ncid, NCI-ncip, and NCI-ncidiv subsets in the Zinc database (http://zinc.docking.org/). A grid 27 Å × 25.5 Å × 14.25 Å was set to circumscribe the target region. The flexibility of the RhoGEF was restricted to the side chain of the K2152 hot spot.

The same computational conditions were used in very recent docking simulations of the A13 lead into the crystal structure of unbound Lbc (PDB: 4D0O) complemented with the missed side chains. Furthermore, AutoDock Vina in full-rigid protein mode was carried out on the 75,000 frames of a 0.75 μs MD trajectory of solvated Lbc achieved by means of GROMACS v4.6.3 (Hess et al., 2008). The 75,000 docking poses were subjected to cluster analysis by means of the GROMOS method and a 2.0 Å Cα-RMSD cutoff. The stability of the best scored and the center complexes in six major clusters was probed by 12 independent MD relaxations, one of which was followed by 60 ns of adaptive temperature MD (Zhang and Ma, 2010). All these MD simulations on the A13-Lbc complex were carried out by NAMD (Phillips et al., 2005).

Details on docking analysis and MD simulations can be found in the Supplemental Information.

In Vitro Experiments

Descriptions of the expression constructs, expression and purification of recombinant proteins in bacteria, cell culture and transfections, GST pull-down, Rhotekin Rho-binding domain and PAK1 Cdc42/Rac1-binding domain pull-down, SDS-PAGE and western blotting, actin stress fiber formation assay, foci formation assay, microscale thermophoresis, SPR, nucleotide-exchange activity, small interfering RNAs, and statistical analysis are provided in the Supplemental Information.

Cell Proliferation Assay

PC-3 cells (1.5×10^5) were seeded on 35 mm coverslips and cultured in RPMI1640 supplemented with 10% fetal bovine serum (FBS). After 24 hr, cells were incubated for an additional 24 hr with 10% FBS and 10 μM bromodeoxyuridine (BrdU) in the absence or presence of 10 μM A13, A2, or Y16 (Shang et al., 2013). The concentration of DMSO in the medium was 0.1% for all experimental conditions. Cells were then washed twice with PBS, fixed for 10 min in PBS/2% paraformaldehyde, and permeabilized for 20 min with 0.25% (w/v) Triton X-100 in PBS. Coverslips were incubated for 10 min with ice-cold 1 N HCl, for 20 min with 2 N HCl at room temperature, and for an additional 20 min with 2 N HCl at 37°C. HCl was then neutralized by two 10 min washes with 0.1 M borate (pH 7.5). Coverslips were blocked for 1 hr in buffer A (10 mM Tris-HCl [pH 7.5], 155 mM NaCl, 2 mM EGTA, 2 mM $MgCl_2$) supplemented with 1% BSA. The incorporation of BrdU was assessed by incubating cells for 2 hr with a 1:200 dilution of the rat anti-BrdU antibody (Sigma) followed by incubation for 1 hr with a 1:250 dilution of Alexa Fluor 488-conjugated anti-rat secondary antibodies (Molecular Probes) and 10 min incubation with DAPI (1 μg/mL). Immunofluorescent staining was visualized using an Advanced Microscopy Group EVOS fluorescence microscope.

Cell Migration: Wound Assays

PC-3 cells (5×10^5) were cultured in 12-well dishes in the presence of RPMI1640 supplemented with 10% FBS. After 24 hr, confluent cell monolayers were wounded with a 1,000 μL tip, washed once with PBS, and cultured for an additional 36 hr in RPMI1640 supplemented with 10% FBS in the absence or presence of 10 μM A13, A2, or Y16. The concentration of DMSO in the medium was 0.1% for all experimental conditions. For RNAi experiments, PC-3 cells were transfected with 25 pmol of control or AKAP-Lbc-specific short hairpin RNAs (shRNAs). Forty-eight hours after transfection, cell monolayers were wounded and cultured for an additional 36 hr in RPMI1640 supplemented with 10% FBS.

Recolonization of the wounded area was imaged every 12 hr with an Advanced Microscopy Group EVOS microscope. The area devoid of cells was measured using ImageJ software.

Cell Migration: Time-Lapse Microscopy Assays

PC-3 cells (3×10^5) were seeded in 12-well dishes in the presence of RPMI1640 containing 10% FBS. After 24 hr, cells were treated in the absence or presence of 10 μM A13 or A2, and random migration was imaged using a time-lapse microscope over a period of 10 hr. The concentration of DMSO in the medium was 0.1% for all experimental conditions. For RNAi experiments, PC-3 cells were transfected with 15 pmol of control or AKAP-Lbc-specific shRNAs. Forty-eight hours after transfection, cell monolayers were imaged as indicated above. Images were taken every 10 min. Migration trajectories and velocities (μm/min) were determined on a total of 160 cells per condition using the Gradientech Tracking Tool software (Gradientech).

Cell Invasion Assays

Invasion assays were performed using a modified Boyden chamber technique that measures the ability of PC-3 cells to migrate across a matrix barrier in the presence of 10% serum. We used 24-well tissue culture plates with inserts containing an 8 μm pore size polycarbonate membrane coated with Matrigel basement membrane matrix (BD Biosciences). PC-3 cells were quiesced in RPMI1640 containing 0.5% FBS for 24 hr. Cells were then trypsinized, resuspended in RPMI1640 containing 0.5% FBS, and counted. A total of 2.5×10^4 cells were loaded into the upper chamber. The lower chamber was filled with RPMI1640 supplemented with 10% FCS. A13 (10 μM), A2 (10 μM), Y16 (10 μM), or DMSO was added both in the upper and lower chambers. The concentration of DMSO in the medium was 0.1% for all experimental conditions. After a 36 hr incubation period, the cell suspension was aspirated, and the membranes were fixed in 70% ethanol at −20°C for 20 min. Cells that had attached but not migrated were removed, the membranes were rinsed in water, and migrated cells on the underside of the membrane were visualized with staining in 2% crystal violet. Cells were counted on three independent transwell membranes using a light microscope.

SUPPLEMENTAL INFORMATION

Supplemental Information includes Supplemental Experimental Procedures, 13 figures, and three tables and can be found with this article online at http://dx.doi.org/10.1016/j.chembiol.2016.07.015.

AUTHOR CONTRIBUTIONS

D.D. conceived, supervised, and in part performed in vitro experiments. F.R. performed all stages of virtual screening. C.D.D.V. performed in vitro screening of compounds, pull-down experiments, transformation assays, and stress fibers formation assays. E.D., E.R., and H.O. performed proliferation, migration, and invasion assays. L.R. performed the initial in vitro screening of compounds and pull-down assays. C.G. and S.C. performed mutagenesis experiments and pull-down assays. C.B. and M.L. performed SPR measurements and GEF activity determinations. M.O. supervised the biophysical studies by C.B. and M.L. M.S. participated in setting and handling compound libraries. L.B. performed docking of A13 on the MD trajectory frames of Lbc as well as MD relaxation of A13-Lbc complexes. F.F. conceived the study, supervised, and in part performed computational experiments and analysis. D.D. and F.F. wrote the manuscript.

ACKNOWLEDGMENTS

This study was supported by AIRC-Italy grants (IG10740 and IG14811) to F.F. and by a Swiss National Science Foundation grant (31003A_156713) to D.D.. M.O. acknowledges support from the Wellcome Trust, MRC, and CAIP. We acknowledge the computer resources from Res Española de Supercomputacion (BCV-2011-2-0011) and CINECA ISCRA A 2011, which served for virtual screening. We acknowledge Monique Nenniger-Tosato for excellent technical assistance and Benjamin Tschumi for his contribution to the GST pull-down experiments. The use of PyMOL 0.99rc6 software for the realization of all drawings is acknowledged. F.R. and C.D.D.V. contributed equally to this work.

Received: September 28, 2014
Revised: June 30, 2016
Accepted: July 9, 2016
Published: September 1, 2016

REFERENCES

Abdul Azeez, K.R., Knapp, S., Fernandes, J.M., Klussmann, E., and Elkins, J.M. (2014). The crystal structure of the RhoA-AKAP-Lbc DH-PH domain complex. Biochem. J. *464*, 231–239.

Aittaleb, M., Boguth, C.A., and Tesmer, J.J. (2009). Structure and function of heterotrimeric G protein-regulated Rho guanine nucleotide exchange factors. Mol. Pharmacol. *77*, 111–125.

Arthur, W.T., Ellerbroek, S.M., Der, C.J., Burridge, K., and Wennerberg, K. (2002). XPLN, a guanine nucleotide exchange factor for RhoA and RhoB, but not RhoC. J. Biol. Chem. *277*, 42964–42972.

Baisamy, L., Jurisch, N., and Diviani, D. (2005). Leucine zipper-mediated homo-oligomerization regulates the Rho-GEF activity of AKAP-Lbc. J. Biol. Chem. *280*, 15405–15412.

Bonuccelli, G., Casimiro, M.C., Sotgia, F., Wang, C., Liu, M., Katiyar, S., Zhou, J., Dew, E., Capozza, F., Daumer, K.M., et al. (2009). Caveolin-1 (P132L), a common breast cancer mutation, confers mammary cell invasiveness and defines a novel stem cell/metastasis-associated gene signature. Am. J. Pathol. *174*, 1650–1662.

Bouquier, N., Fromont, S., Zeeh, J.C., Auziol, C., Larrousse, P., Robert, B., Zeghouf, M., Cherfils, J., Debant, A., and Schmidt, S. (2009a). Aptamer-derived peptides as potent inhibitors of the oncogenic RhoGEF Tgat. Chem. Biol. *16*, 391–400.

Bouquier, N., Vignal, E., Charrasse, S., Weill, M., Schmidt, S., Leonetti, J.P., Blangy, A., and Fort, P. (2009b). A cell active chemical GEF inhibitor selectively targets the Trio/RhoG/Rac1 signaling pathway. Chem. Biol. *16*, 657–666.

Bowers, E.M., Yan, G., Mukherjee, C., Orry, A., Wang, L., Holbert, M.A., Crump, N.T., Hazzalin, C.A., Liszczak, G., Yuan, H., et al. (2010). Virtual ligand screening of the p300/CBP histone acetyltransferase: identification of a selective small molecule inhibitor. Chem. Biol. *17*, 471–482.

Brown, L.M., Rogers, K.E., Aroonsakool, N., McCammon, J.A., and Insel, P.A. (2014). Allosteric inhibition of Epac: computational modeling and experimental validation to identify allosteric sites and inhibitors. J. Biol. Chem. *289*, 29148–29157.

Cardama, G.A., Comin, M.J., Hornos, L., Gonzalez, N., Defelipe, L., Turjanski, A.G., Alonso, D.F., Gomez, D.E., and Menna, P.L. (2014). Preclinical development of novel Rac1-GEF signaling inhibitors using a rational design approach in highly aggressive breast cancer cell lines. Anticancer Agents Med. Chem. *14*, 840–851.

Chikumi, H., Barac, A., Behbahani, B., Gao, Y., Teramoto, H., Zheng, Y., and Gutkind, J.S. (2004). Homo- and hetero-oligomerization of PDZ-RhoGEF, LARG and p115RhoGEF by their C-terminal region regulates their in vivo Rho GEF activity and transforming potential. Oncogene *23*, 233–240.

Colicelli, J. (2004). Human RAS superfamily proteins and related GTPases. Sci. STKE *2004*, RE13.

Cook, D.R., Rossman, K.L., and Der, C.J. (2013). Rho guanine nucleotide exchange factors: regulators of Rho GTPase activity in development and disease. Oncogene *33*, 4021–4035.

Diviani, D., Soderling, J., and Scott, J.D. (2001). AKAP-Lbc anchors protein kinase A and nucleates Galpha 12-selective Rho-mediated stress fiber formation. J. Biol. Chem. *276*, 44247–44257.

Diviani, D., Abuin, L., Cotecchia, S., and Pansier, L. (2004). Anchoring of both PKA and 14-3-3 inhibits the Rho-GEF activity of the AKAP-Lbc signaling complex. EMBO J. *23*, 2811–2820.

Evelyn, C.R., Duan, X., Biesiada, J., Seibel, W.L., Meller, J., and Zheng, Y. (2014). Rational design of small molecule inhibitors targeting the Ras GEF, SOS1. Chem. Biol. *21*, 1618–1628.

Feher, L.Z., Pocsay, G., Krenacs, L., Zvara, A., Bagdi, E., Pocsay, R., Lukacs, G., Gyory, F., Gazdag, A., Tarko, E., and Puskas, L.G. (2012). Amplification of thymosin beta 10 and AKAP13 genes in metastatic and aggressive papillary thyroid carcinomas. Pathol. Oncol. Res. *18*, 449–458.

Friesland, A., Zhao, Y., Chen, Y.H., Wang, L., Zhou, H., and Lu, Q. (2013). Small molecule targeting Cdc42-intersectin interaction disrupts Golgi organization and suppresses cell motility. Proc. Natl. Acad. Sci. USA *110*, 1261–1266.

Fukuhara, S., Murga, C., Zohar, M., Igishi, T., and Gutkind, J.S. (1999). A novel PDZ domain containing guanine nucleotide exchange factor links heterotrimeric G proteins to Rho. J. Biol. Chem. *274*, 5868–5879.

Fukuhara, S., Chikumi, H., and Gutkind, J.S. (2000). Leukemia-associated Rho guanine nucleotide exchange factor (LARG) links heterotrimeric G proteins of the G(12) family to Rho. FEBS Lett. *485*, 183–188.

Gao, Y., Dickerson, J.B., Guo, F., Zheng, J., and Zheng, Y. (2004). Rational design and characterization of a Rac GTPase-specific small molecule inhibitor. Proc. Natl. Acad. Sci. USA *101*, 7618–7623.

Gu, J., Wu, X., Dong, Q., Romeo, M.J., Lin, X., Gutkind, J.S., and Berman, D.M. (2006). A nonsynonymous single-nucleotide polymorphism in the PDZ-Rho guanine nucleotide exchange factor (Ser1416Gly) modulates the risk of lung cancer in Mexican Americans. Cancer *106*, 2716–2724.

Hart, M.J., Sharma, S., elMasry, N., Qiu, R.G., McCabe, P., Polakis, P., and Bollag, G. (1996). Identification of a novel guanine nucleotide exchange factor for the Rho GTPase. J. Biol. Chem. *271*, 25452–25458.

Hart, M.J., Jiang, X., Kozasa, T., Roscoe, W., Singer, W.D., Gilman, A.G., Sternweis, P.C., and Bollag, G. (1998). Direct stimulation of the guanine nucleotide exchange activity of p115 RhoGEF by Galpha13. Science *280*, 2112–2114.

Hess, B., Kutzner, C., Van Der Spoel, D., and Lindahl, E. (2008). GROMACS 4: algorithms for highly efficient, load-balanced, and scalable molecular simulation. J. Chem. Theory Comput. *4*, 435–447.

Hodge, J.C., Bub, J., Kaul, S., Kajdacsy-Balla, A., and Lindholm, P.F. (2003). Requirement of RhoA activity for increased nuclear factor kappaB activity and PC-3 human prostate cancer cell invasion. Cancer Res. *63*, 1359–1364.

Hu, J.K., Wang, L., Li, Y., Yang, K., Zhang, P., Chen, X.Z., Wang, R., and Zhou, Z.G. (2010). The mRNA and protein expression of A-kinase anchor proteins 13 in human colorectal cancer. Clin. Exp. Med. *10*, 41–49.

Huang, C., Liu, S., and Miller, R.T. (2011). Role of p115RhoGEF in the regulation of extracellular Ca(2+)-induced choline kinase activation and prostate cancer cell proliferation. Int. J. Cancer *128*, 2833–2842.

Jaffe, A.B., and Hall, A. (2005). Rho GTPases: biochemistry and biology. Annu. Rev. Cell Dev. Biol. *21*, 247–269.

Jaiswal, M., Gremer, L., Dvorsky, R., Haeusler, L.C., Cirstea, I.C., Uhlenbrock, K., and Ahmadian, M.R. (2011). Mechanistic insights into specificity, activity, and regulatory elements of the regulator of G-protein signaling (RGS)-containing Rho-specific guanine nucleotide exchange factors (GEFs) p115, PDZ-RhoGEF (PRG), and leukemia-associated RhoGEF (LARG). J. Biol. Chem. *286*, 18202–18212.

Jaiswal, M., Dvorsky, R., and Ahmadian, M.R. (2013). Deciphering the molecular and functional basis of Dbl family proteins: a novel systematic approach toward classification of selective activation of the Rho family proteins. J. Biol. Chem. *288*, 4486–4500.

Karlsson, R., Pedersen, E.D., Wang, Z., and Brakebusch, C. (2009). Rho GTPase function in tumorigenesis. Biochim. Biophys. Acta *1796*, 91–98.

Kristelly, R., Gao, G., and Tesmer, J.J. (2004). Structural determinants of RhoA binding and nucleotide exchange in leukemia-associated Rho guanine-nucleotide exchange factor. J. Biol. Chem. *279*, 47352–47362.

Lewis, T.E., Milam, T.D., Klingler, D.W., Rao, P.S., Jaggi, M., Smith, D.J., Hemstreet, G.P., and Balaji, K.C. (2005). Tissue transglutaminase interacts with protein kinase A anchor protein 13 in prostate cancer. Urol. Oncol. *23*, 407–412.

Muller, J.M., Metzger, E., Greschik, H., Bosserhoff, A.K., Mercep, L., Buettner, R., and Schule, R. (2002). The transcriptional coactivator FHL2 transmits Rho signals from the cell membrane into the nucleus. EMBO J. *21*, 736–748.

Phillips, J.C., Braun, R., Wang, W., Gumbart, J., Tajkhorshid, E., Villa, E., Chipot, C., Skeel, R.D., Kale, L., and Schulten, K. (2005). Scalable molecular dynamics with NAMD. J. Comput. Chem. *26*, 1781–1802.

Raponi, M., Harousseau, J.L., Lancet, J.E., Lowenberg, B., Stone, R., Zhang, Y., Rackoff, W., Wang, Y., and Atkins, D. (2007). Identification of molecular predictors of response in a study of tipifarnib treatment in relapsed and refractory acute myelogenous leukemia. Clin. Cancer Res. *13*, 2254–2260.

Rolland, D., Ribrag, V., Haioun, C., Ghesquieres, H., Jardin, F., Bouabdallah, R., Franchi, P., Briere, J., De Kerviler, E., Chassagne-Clement, C., et al. (2010). Phase II trial and prediction of response of single agent tipifarnib in patients with relapsed/refractory mantle cell lymphoma: a Groupe d'Etude des Lymphomes de l'Adulte trial. Cancer Chemother. Pharmacol. *65*, 781–790.

Rossman, K.L., Der, C.J., and Sondek, J. (2005). GEF means go: turning on Rho GTPases with guanine nucleotide-exchange factors. Nat. Rev. Mol. Cell Biol. *6*, 167–180.

Sali, A., and Blundell, T.L. (1993). Comparative protein modelling by satisfaction of spatial restraints. J. Mol. Biol. *234*, 779–815.

Schmidt, L.J., Duncan, K., Yadav, N., Regan, K.M., Verone, A.R., Lohse, C.M., Pop, E.A., Attwood, K., Wilding, G., Mohler, J.L., et al. (2012). RhoA as a mediator of clinically relevant androgen action in prostate cancer cells. Mol. Endocrinol. *26*, 716–735.

Senapati, S., Rachagani, S., Chaudhary, K., Johansson, S.L., Singh, R.K., and Batra, S.K. (2010). Overexpression of macrophage inhibitory cytokine-1 induces metastasis of human prostate cancer cells through the FAK-RhoA signaling pathway. Oncogene *29*, 1293–1302.

Shang, X., Marchioni, F., Sipes, N., Evelyn, C.R., Jerabek-Willemsen, M., Duhr, S., Seibel, W., Wortman, M., and Zheng, Y. (2012). Rational design of small molecule inhibitors targeting RhoA subfamily Rho GTPases. Chem. Biol. *19*, 699–710.

Shang, X., Marchioni, F., Evelyn, C.R., Sipes, N., Zhou, X., Seibel, W., Wortman, M., and Zheng, Y. (2013). Small-molecule inhibitors targeting G-protein-coupled Rho guanine nucleotide exchange factors. Proc. Natl. Acad. Sci. USA *110*, 3155–3160.

Somlyo, A.V., Bradshaw, D., Ramos, S., Murphy, C., Myers, C.E., and Somlyo, A.P. (2000). Rho-kinase inhibitor retards migration and in vivo dissemination of human prostate cancer cells. Biochem. Biophys. Res. Commun. *269*, 652–659.

Sterpetti, P., Marucci, L., Candelaresi, C., Toksoz, D., Alpini, G., Ugili, L., Baroni, G.S., Macarri, G., and Benedetti, A. (2006). Cell proliferation and drug resistance in hepatocellular carcinoma are modulated by Rho GTPase signals. Am. J. Physiol. Gastrointest. Liver Physiol. *290*, G624–G632.

Toksoz, D., and Williams, D.A. (1994). Novel human oncogene lbc detected by transfection with distinct homology regions to signal transduction products. Oncogene *9*, 621–628.

Trott, O., and Olson, A.J. (2010). Software news and update AutoDock Vina: improving the speed and accuracy of docking with a new scoring function, efficient optimization, and multithreading. J. Comput. Chem. *31*, 455–461.

Vives, V., Laurin, M., Cres, G., Larrousse, P., Morichaud, Z., Noel, D., Cote, J.F., and Blangy, A. (2011). The Rac1 exchange factor Dock5 is essential for bone resorption by osteoclasts. J. Bone Miner. Res. *26*, 1099–1110.

Wang, Q., Liu, M., Kozasa, T., Rothstein, J.D., Sternweis, P.C., and Neubig, R.R. (2004). Thrombin and lysophosphatidic acid receptors utilize distinct rhoGEFs in prostate cancer cells. J. Biol. Chem. *279*, 28831–28834.

Ward, Y., Lake, R., Yin, J.J., Heger, C.D., Raffeld, M., Goldsmith, P.K., Merino, M., and Kelly, K. (2011). LPA receptor heterodimerizes with CD97 to amplify LPA-initiated RHO-dependent signaling and invasion in prostate cancer cells. Cancer Res. *71*, 7301–7311.

Wirtenberger, M., Tchatchou, S., Hemminki, K., Klaes, R., Schmutzler, R.K., Bermejo, J.L., Chen, B., Wappenschmidt, B., Meindl, A., Bartram, C.R., and Burwinkel, B. (2006). Association of genetic variants in the Rho guanine nucleotide exchange factor AKAP13 with familial breast cancer. Carcinogenesis *27*, 593–598.

Zhang, C., and Ma, J. (2010). Enhanced sampling and applications in protein folding in explicit solvent. J. Chem. Phys. *132*, 244101.

Zhang, C., Zhang, S., Zhang, Z., He, J., Xu, Y., and Liu, S. (2013). ROCK has a crucial role in regulating prostate tumor growth through interaction with c-Myc. Oncogene *33*, 5582–5591.

Zheng, Y., Olson, M.F., Hall, A., Cerione, R.A., and Toksoz, D. (1995). Direct involvement of the small GTP-binding protein Rho in lbc oncogene function. J. Biol. Chem. *270*, 9031–9034.